Heat Transfer Research 45(6), 563–578 (2014)

MIXED-CONVECTION FLOW IN A LID-DRIVEN SQUARE CAVITY FILLED WITH A NANOFLUID WITH VARIABLE PROPERTIES: EFFECT OF THE NANOPARTICLE DIAMETER AND OF THE POSITION OF A HOT OBSTACLE

Mohammad Hemmat Esfe, Seyed Sadegh Mirtalebi Esforjani, Mohammad Akbari, & Arash Karimipour*

Department of Mechanical Engineering, Najafabad Branch, Islamic Azad University, Isfahan, Iran

*Address all correspondence to Mohammad Hemmat Esfe
E-mail: M.hemmatesfe@gmail.com

In this article, a mixed-convection flow in a cavity filled with an Al_2O_3/water nanofluid and having an inside hot obstacle and variable properties is studied numerically using the finite volume method. The thermal conductivity and effective viscosity of the nanofluid were determined using the new variable properties models proposed by Xu and Jang, respectively. The bottom, top, and the left walls of the cavity are adiabatic, while the right wall is maintained at a cold temperature (T_c). A hot rectangular obstacle is located at the bottom of the square cavity. The upper adiabatic lid is moving in its positive direction. To numerically solve the governing equations, the finite volume method along with a displaced grid system is used, and the equations are transformed into a code using FORTRAN. In this study the influence of some important parameters such as the diameter of a nanoparticle, Richardson number, and the position of the hot obstacle on the hydrodynamic and thermal characteristics are discussed. The results indicate that a decrease in the nanoparticle diameter at a constant Ri enhances heat transfer. On the other hand, the heat transfer rate increased as Ri was decreased for a particular diameter and position of the hot obstacle.

KEY WORDS: *nanofluid, variable properties, solid volume fraction, hot obstacle*

1. INTRODUCTION

Nanofluids are produced by suspending nanometer-sized particles (less than 100 nm) in a pure fluid such as water, ethylene glycol or propylene glycol. The first to coin the "nanofluids" for these fluids with superior thermal properties was Choi (1995). The existence of high thermal conductivity metallic nanoparticles (e.g., copper, aluminum, silver, and titanium) increases the thermal conductivity of such mixtures, thus enhancing their overall heat transfer capability (Xuan et al., 2003). In recent years, nanofluids have attracted attention as an innovation in using heat transfer fluids in the

1064-2285/14/$35.00 © 2014 by Begell House, Inc.

NOMENCLATURE

c_p	specific heat, $J \cdot kg^{-1} \cdot K^{-1}$
Gr	Grashof number
g	gravitational acceleration, $m \cdot s^{-2}$
h	heat transfer coefficient, $W \cdot m^{-2} \cdot K^{-1}$
L	enclosure length, m
k	thermal conductivity, $W \cdot m^{-1} \cdot K^{-1}$
Nu	Nusselt number
p	pressure, $N \cdot m^{-2}$
P	dimensionless pressure
Pr	Prandtl number
q	heat flux, $W \cdot m^{-2}$
Re	Reynolds number
Ri	Richardson number
T	dimensional temperature, K
u, v	dimensional velocity components in the x and y directions, $m \cdot s^{-1}$
U, V	dimensionless velocity components in the X and Y directions
U_0	lid velocity
x, y	dimensional Cartesian coordinates, m
X, Y	dimensionless Cartesian coordinates

Greek symbols

α	thermal diffusivity, $m^2 \cdot s$
β	thermal expansion coefficient, K^{-1}
θ	dimensionless temperature
μ	dynamic viscosity, $kg \cdot m^{-1} \cdot s^{-1}$
ν	kinematic viscosity, $m^2 \cdot s^{-1}$
ρ	density, $kg \cdot m^{-3}$
φ	volume fraction of nanoparticles

Subscripts

c	cold
eff	effective
f	fluid
h	hot
nf	nanofluid
s	solid particles
w	wall

heating of buildings, in various heat exchangers, in plants, and in automotive cooling applications, because of their excellent thermal performance. Various benefits from the application of nanofluids include: improved heat transfer, heat transfer system size reduction, minimal clogging, microchannel cooling, and miniaturization of systems (Choi, 1995).

Numerous investigations have been conducted on the thermophysical properties of nanofluids (effective dynamic viscosity, thermal conductivity, etc.) and the energy transport in nanofluids. Studies of the thermophysical properties of nanofluids were carried out by Lee et al. (2001), Xie et al. (2002), Patel et al. (2005), and Chang et al. (2005). Also many theoretical, numerical, and experimental studies on the influence of the existence of nanoparticles on convective heat transfer have been reported.

On the other hand, fluid flow and heat transfer in a cavity filled by a pure fluid which is driven by buoyancy and shear have been studied extensively in the literature. Mixed convection (a kind of convection including both natural and forced convection)

has a significant role in many applications in industry and engineering: lakes and reservoirs (Imberger and Hamblin, 1982), food processing, crystal growth (Moallemi and Jang, 1992), electronic cooling devices, drying technologies, solar ponds (Cha and Jaluria, 1984), solar collectors (Ideriah, 1980), and float glass production (Pilkington, 1969), to cite but a few.

Several investigations on mixed convection in single or double lid-driven enclosure flow and heat transfer including different cavity geometries and configurations, different base fluids and boundary conditions have been reported. Particularly in recent years some interesting researches have been done such as by Saedodin et al. (2011), Abu-Nada and Chamkha (2010), Fereidoon et al. (2013), Zarei et al. (2013), and Abbasian Arani et al. (2012).

Another work that was done by Nikfar and Mahmoodi (2012) also verified the above statement. They studied natural convection in a square cavity filled with an Al_2O_3–water nanofluid. The horizontal walls of the cavity were insulated, while the left and right wavy side walls of the cavity were maintained at high and low constant temperatures. They demonstrated that an increase in the volume fraction of nanoparticles increases the average Nusselt number of the hot wall.

The effect of the existence of an obstacle within the cavity is one of the interesting challenges for researchers. Recently a free-convection fluid flow and heat transfer were investigated numerically by Mahmoodi and Mazrouei Sebdani (2012). Their work dealt with a Cu–water nanofluid around adiabatic square bodies at the center of a square cavity. They showed that for the majority of Rayleigh numbers the Nusselt number increases with the volume fraction of the nanoparticles. They also showed that at low Rayleigh numbers on increase in the size of the adiabatic square body, the rate of heat transfer decreases and that the opposite is true for high Rayleigh numbers.

Mixed convection of an Al_2O_3–water nanofluid in a cavity with a hot moving bottom wall and cold right, left, and top walls was investigated numerically by Mahmoodi (2011). Also, the effect of the nanofluid variable properties on mixed convection in a rectangular cavity was analyzed by Mazrouei Sebdani et al. (2012).

Motivated by the investigations mentioned above, the purpose of the present work was to consider mixed-convection flows of an Al_2O_3–water nanofluid in a square cavity with an inside heated obstacle and an upper lid moving uniformly in the horizontal plane. Also, the effects of the Richardson number, height of the hot obstacle, position of the hot obstacle on the bottom wall, and the solid volume fraction of the Al_2O_3 nanoparticles on the flow and thermal fields and heat transfer inside the cavity are studied.

2. MATHEMATICAL MODELING

Figure 1 shows a two-dimensional square cavity, considered in the present study, with physical dimensions. The cavity is filled with an Al_2O_3–water nanofluid and has an

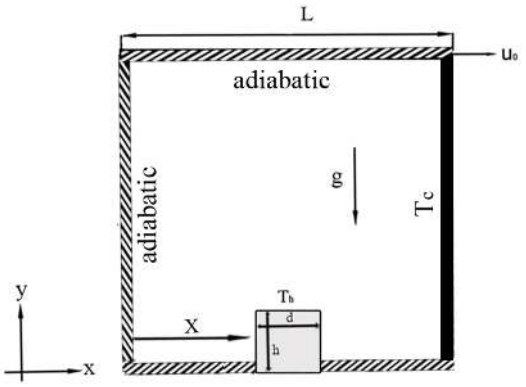

FIG. 1: Schematic diagram of current study

adiabatic upper moving lid. The bottom, top, and left walls are adiabatic, while the right wall is maintained at a low temperature (T_c). A hot rectangular obstacle is located on the bottom wall of the square cavity. The height and the width of this obstacle are denoted by h and d. The distance between the left wall and the hot obstacle is denoted by X. The length of the cavity perpendicular to its plane is assumed to be long enough; hence, the study is considered two-dimensional.

The cavity is filled with a suspension of Al_2O_3 nanoparticles in water without slip between them. The nanofluid is assumed to be incompressible, with the nanoparticles and the base fluid being in thermal equilibrium. The thermophysical properties of the nanoparticles and water as the base fluid at $T = 25^{\circ}C$ are presented in Table 1.

The governing equations for a steady, two-dimensional laminar and incompressible flow are expressed as

$$\frac{\partial u}{\partial x} + \frac{\partial v}{\partial y} = 0 \,, \tag{1}$$

$$u\,\frac{\partial u}{\partial x} + v\,\frac{\partial u}{\partial y} = -\,\frac{1}{\rho_{nf}}\,\frac{\partial p}{\partial x} + \upsilon_{nf}\nabla^2 u \,, \tag{2}$$

TABLE 1: Thermophysical properties of water and Al_2O_3

Solid (Al_2O_3)	Fluid phase (Water)	Physical properties
765	4179	C_p, J/kg·k
3970	997.1	ρ, kg/m^3
25	0.6	K, W·m^{-1}·K^{-1}
0.85	21.	$\beta \times 10^{-5}$, 1/K
……..	8.9	$\mu \times 10^{-4}$, kg/ms

$$u\frac{\partial v}{\partial x}+v\frac{\partial v}{\partial y}=-\frac{1}{\rho_{nf}}\frac{\partial p}{\partial y}+\upsilon_{nf}\nabla^2 v+\frac{(\rho\beta)_{nf}}{\rho_{nf}}g\Delta T\ , \tag{3}$$

and

$$u\frac{\partial T}{\partial x}+v\frac{\partial T}{\partial y}=\alpha_{nf}\nabla^2 T\ . \tag{4}$$

The dimensionless parameters may be presented as

$$\begin{gathered}X=\frac{x}{L}\ ,\quad Y=\frac{y}{L}\ ,\quad V=\frac{v}{u_0}\ ,\quad U=\frac{u}{u_0}\ ,\\ \Delta T=T_h-T_c,\quad \theta=\frac{T-T_c}{\Delta T}\ ,\quad P=\frac{p}{\rho_{nf}u_0^2}\ .\end{gathered} \tag{5}$$

Hence,

$$\mathrm{Re}=\frac{\rho_f u_0 L}{\mu_f}\ ,\quad \mathrm{Ri}=\frac{\mathrm{Ra}}{\mathrm{Pr}\ \mathrm{Re}^2}\ ,\quad \mathrm{Ra}=\frac{g\beta_f\Delta T L^3}{\upsilon_f\alpha_f}\ ,\quad \mathrm{Pr}=\frac{\upsilon_f}{\alpha_f}\ . \tag{6}$$

The dimensionless form of the above governing equations, (1) to (4), becomes

$$\frac{\partial U}{\partial X}+\frac{\partial V}{\partial Y}=0\ , \tag{7}$$

$$U\frac{\partial U}{\partial X}+V\frac{\partial U}{\partial Y}=-\frac{\partial P}{\partial X}+\frac{\upsilon_{nf}}{\upsilon_f}\frac{1}{\mathrm{Re}}\nabla^2 U\ , \tag{8}$$

$$U\frac{\partial V}{\partial X}+V\frac{\partial V}{\partial Y}=-\frac{\partial P}{\partial Y}+\frac{\upsilon_{nf}}{\upsilon_f}\frac{1}{\mathrm{Re}}\nabla^2 V+\frac{Ri}{\mathrm{Pr}}\cdot\frac{\beta_{nf}}{\beta_f}\Delta\theta\ , \tag{9}$$

and

$$U\frac{\partial\theta}{\partial X}+V\frac{\partial\theta}{\partial Y}=\frac{\alpha_{nf}}{\alpha_f}\nabla^2\theta\ . \tag{10}$$

2.1 Thermal Diffusivity and Effective Density

The thermal diffusivity and effective density of the nanofluid are

$$\alpha_{nf}=\frac{k_{nf}}{(\rho c_p)_{nf}}\ , \tag{11}$$

$$\rho_{nf}=\varphi\rho_s+(1-\varphi)\rho_f\ . \tag{12}$$

2.2 Heat Capacity and Thermal Expansion Coefficient

Heat capacity and thermal expansion coefficient of the nanofluid therefore are

$$(\rho c_p)_{nf} = \varphi(\rho c_p)_s + (1-\varphi)(\rho c_p)_f, \tag{13}$$

$$(\rho\beta)_{nf} = \varphi(\rho\beta)_s + (1-\varphi)(\rho\beta)_f. \tag{14}$$

2.3 Viscosity

The effective viscosity of nanofluid was calculated by

$$\mu_{eff} = \mu_f(1+2.5\varphi)\left[1+\eta\left(\frac{d_p}{L}\right)^{-2\varepsilon}\varphi^{2/3}(\varepsilon+1)\right]. \tag{15}$$

This well-validated model is presented by Jang et al. (2013) for a fluid containing a dilute suspension of small rigid spherical particles, and it accounts for the slip mechanism in nanofluids. The empirical constants ε and η are –0.25 and 280 for Al_2O_3, respectively.

It is worth mentioning that the viscosity of the base fluid (water) is considered to vary with temperature and the flowing equation is used to evaluate the viscosity of water:

$$\mu_{H_2O} = (1.2723\times T_{rc}{}^5 - 8.736\times T_{rc}{}^4 + 33.708\times T_{rc}{}^3 - 246.6\times T_{rc}{}^2 + 518.78\times T_{rc} + 1153.9)\times 10^6, \tag{16a}$$

where

$$T_{rc} = \log(T-273). \tag{16b}$$

2.4 Dimensionless Stagnant Thermal Conductivity

The effective thermal conductivity of the nanoparticles in the liquid as stationary is calculated by the Hamilton and Crosser (1962) (H–C model), which is

$$\frac{k_{\text{stationary}}}{k_f} = \frac{k_s + 2k_f - 2\varphi(k_f - k_s)}{k_s + 2k_f + \varphi(k_f - k_s)}. \tag{17}$$

2.5 Total Dimensionless Thermal Conductivity of Nanofluids

$$\frac{k_{nf}}{k_f} = \frac{k_{\text{stationary}}}{k_f} + \frac{k_c}{k_f} = \frac{k_s + 2k_f - 2\varphi(k_f - k_s)}{k_s + 2k_f + \varphi(k_f - k_s)} + c\,\frac{Nu_p d_f \left(2 - D_f\right) D_f}{\text{Pr}\left(1 - D_f\right)^2} \frac{\left[\left(\frac{d_{\max}}{d_{\min}}\right)^{1-Df} - 1\right]^2}{\left(\frac{d\ \max}{d\ \min}\right)^{2-Df} - 1} \frac{1}{d_p} \quad . \tag{18}$$

This model was proposed by Xu et al. (2006) and it has been chosen in this study to describe the thermal conductivity of nanofluids. Here c is an empirical constant (e.g., $c = 85$ for deionized water and $c = 280$ for ethylene glycol) which is independent of the type of nanoparticles. Nu_p is the Nusselt number for a liquid flowing around a spherical particle and equal to two for a single particle in this work. The fluid molecular diameter $d_\text{f} = 0.45$ nm for water in present study. The fractal dimension D_f is determined by

$$D_f = 2 - \frac{\ln \varphi}{\ln\left(\frac{d_{p,\min}}{d_{p,\max}}\right)}, \tag{19}$$

$$d_{p,\max} = d_p \frac{D_f - 1}{D_f}\left(\frac{d_{p,\min}}{d_{p,\max}}\right)^{-1}, \qquad d_{p,\min} = d_p \frac{D_f - 1}{D_f}, \tag{20}$$

where $d_{p,\max}$ and $d_{p,\min}$ are the maximum and minimum diameters of nanoparticles, respectively. The ratio of minimum to maximum nanoparticles $d_{p,\min}/d_{p,\max}$ is R. In this study, R is constant and equal to 0.007.

3. NUMERICAL IMPLEMENTATION

The governing equations (including continuity, momentum, and energy equations) are discretized using the finite volume method with a staggered grid system. The SIMPLER algorithm has been adopted for the pressure velocity coupling. The convection terms are approximated by a blend of the central difference scheme with the upwind scheme (hybrid scheme) which is conducive to a stable solution. Besides, a second-or-

der central differencing scheme is used for the diffusion terms. The algebraic system arising from the numerical discretization is computed using the Tridiagonal Matrix Algorithm (TDMA). The solution process is repeated until an acceptable convergence criterion is reached. A FORTRAN computer code has been developed to solve the equations as described above. The process is repeated until the following convergence criterion is satisfied:

$$\text{error} = \frac{\sum_{j=1}^{j=M}\sum_{i=1}^{i=N}\left|\lambda^{n+1}-\lambda^{n}\right|}{\sum_{j=1}^{j=M}\sum_{i=1}^{i=N}\left|\lambda^{n+1}\right|} < 10^{-7}. \tag{21}$$

Here, M and N correspond to the number of grid points in the x and y directions, respectively, n is the number of iteration, and λ denotes any scalar transport quantity.

To verify the grid independence, the numerical procedure was carried out for 11 different mesh sizes. The average Nu of the hot body wall at $X = 0.4L$, Ri = 0.1, $h = 0.2L$, and $\varphi = 0.03$ is obtained for each grid size as shown in Fig 2.

As can be seen, an 101 × 101 uniform grid size yields the required accuracy and was hence applied for all simulation exercises in this work as presented in the following section.

To ensure the accuracy and validity of this new model, we analyze a square cavity filled with a base fluid at different Re and Ri numbers. Table 2 shows the comparison between the results obtained with our new model and the values presented in the literature. The quantitative comparisons for the average Nusselt numbers indicate an excellent agreement between them.

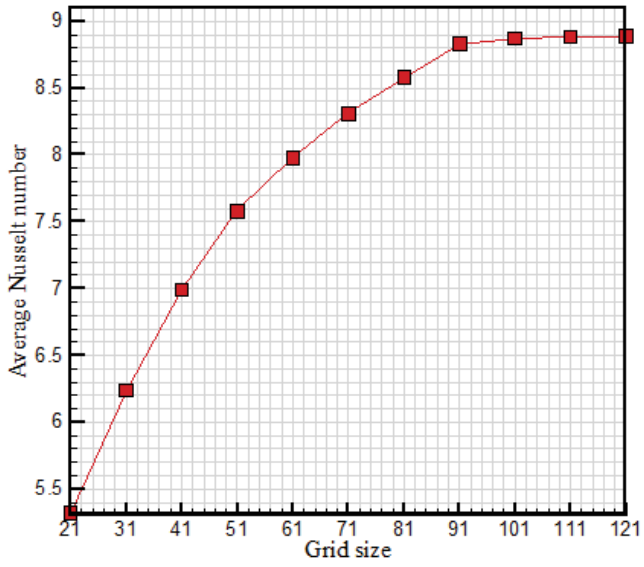

FIG. 2: Average Nusselt number for different uniform grids

TABLE 2: Comparison between the results of the present study with the results of other researches

Re	Ri	Present study (101 × 101)	Abu-Nada et al. (2010)	Waheed (2009)	Tiwari and Das (2007)	Abdel-khalek (2008)	Khanafer et al. (2007)	Sharif (2007)
1	100	0.9914	1.010134	1.00033	–	–	–	–
100	0.01	2.0169	2.090837	2.03116	2.10	1.985	2.02	
400	0.000625	3.90	4.162057	4.02462	3.85	3.8785	4.01	4.05
500	0.0004	4.4760	4.663689	4.52671	–	–	–	–
1000	0.0001	6.3907	6.551615	6.48423	6.33	6.345	6.42	6.55

4. RESULTS AND DISCUSSION

In this paper, heat transfer inside a square cavity filled with a nanofluid is studied relying on streamlines and isotherms plots as well as Nusselt number diagrams. All diagrams are plotted assuming that $Gr = 10^4$ and that the nanofluid has a temperature and volume fraction of 300° and 0.05, respectively. The obstacle height is also assumed to be constant and equal to $0.1L$.

Variation of the isothermal lines and streamlines at different diameters of the nanoparticles dispersed in water is illustrated in Fig. 3 at Ri = 1 and $X = 0.4L$. As inferred from the streamlines in this range of parameters and at all diameters, a primary clockwise cell produced by the shear force of the top moving lid and buoyancy force due to the fluid temperature difference occupies almost the whole cavity. The intensity and shape of this cell at all the diameters studied are approximately the same, whereas a changing nanoparticle diameter practically has no effect on the flow condition. The isothermal lines also show the presence of a thermal boundary layer at the boundaries of the warm walls. The isothermal lines near the hot walls are very dense indicating a high temperature gradient and heat transfer rate there. By precise analysis of temperature diagrams, it is inferred that as the nanoparticle diameter increases, the isothermal lines near the isothermal walls slightly become less crowded and, therefore, it is expected that this reduction in the temperature gradient causes the Nusselt number and total heat transfer inside the cavity to reduce.

Variation of the thermal and fluid flow behaviors as a function of a changing Richardson number inside the cavity filled with a nanofluid at $d_p = 40$ nm and $x = 0.2L$ is shown in Fig. 4. The flow pattern at Ri = 0.1 indicates the formation of a central clockwise vortex inside the cavity. The form of this vortex does not change significantly on changing the Richardson number. As the Richardson number increases, the

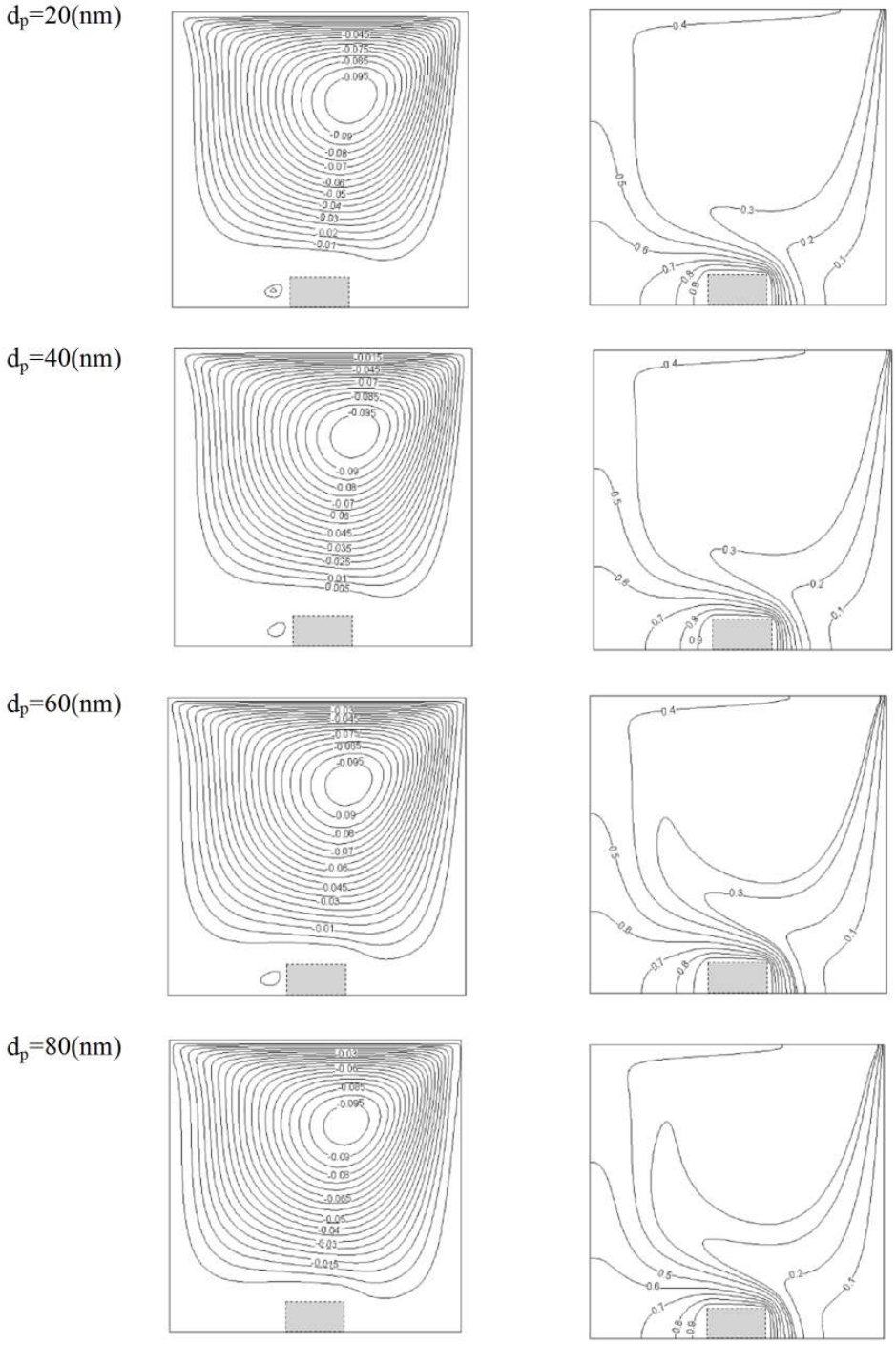

FIG. 3: Streamlines (on the left) and isotherms (on the right) at Ri = 1, $X = 0.4L$ for different diameters of nanoparticles

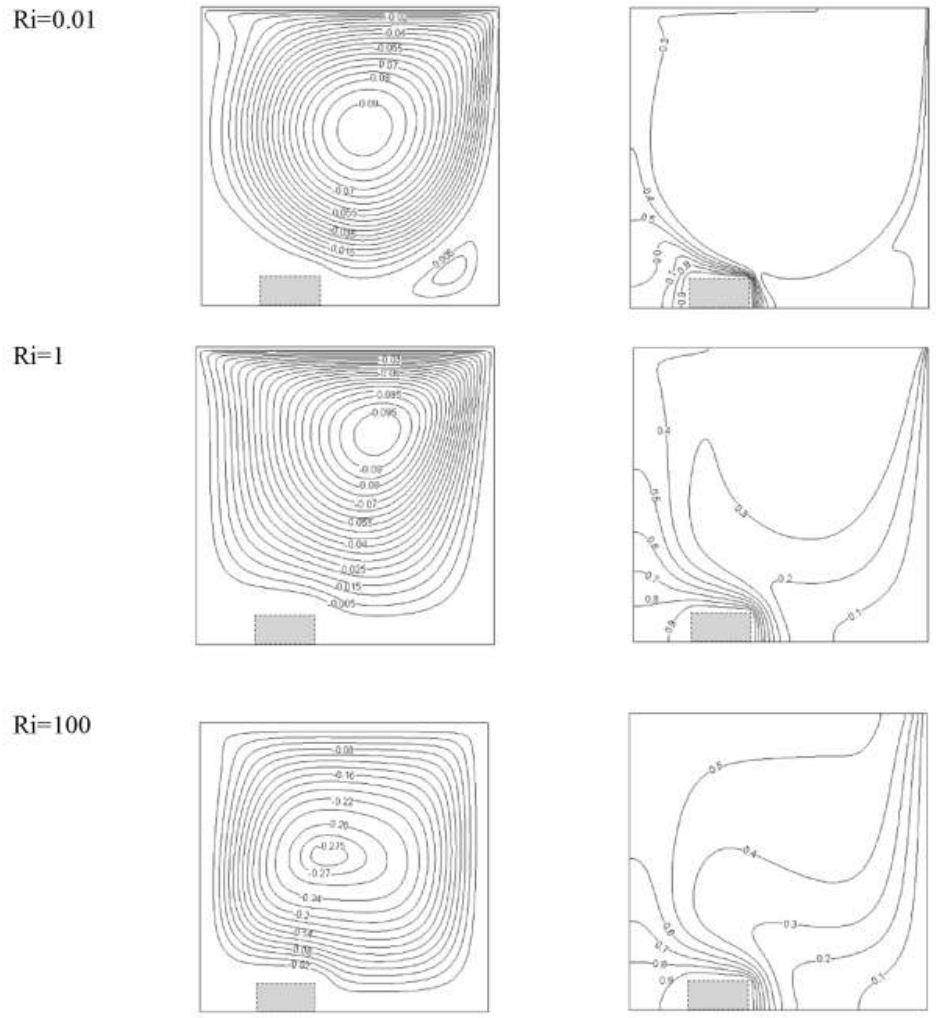

FIG. 4: Streamlines (on the left) and isotherms (on the right) at d_p = 40 nm and $x = 0.2L$ for different Richardson numbers

central vortex is weakened and its intensity is reduced. In addition, with an increasing Richardson number, the buoyancy force dominates the shear force and few deflections in the top left corner of the vortex are modified and the vortex becomes approximately symmetric. The crowded isothermal lines near the hot obstacle walls at Ri = 0.1 indicate intense forced convection in this condition. With an increasing Richardson number, the isothermal lines become less dense, the temperature gradient near the isothermal walls is reduced, and the isothermal lines are separated from each other. At higher Richardson numbers, heat exchange also occurs at the center of the cavity.

Variation of the isothermal lines and streamlines inside the cavity versus changes in the position of the hot obstacle on the bottom wall is demonstrated in Fig. 5. All streamlines and isotherms are plotted for d_p = 40 nm, $\varphi = 0.05$, and T = 300°. Despite the fact that different surfaces of the obstacle are exposed to the nanofluid flow but as the position of the obstacle over cavity bottom wall changes, no significant change occurs in the flow pattern. This is clearly observed in the figures demonstrating isothermal lines. As the hot obstacle is moved further apart from the left wall, the

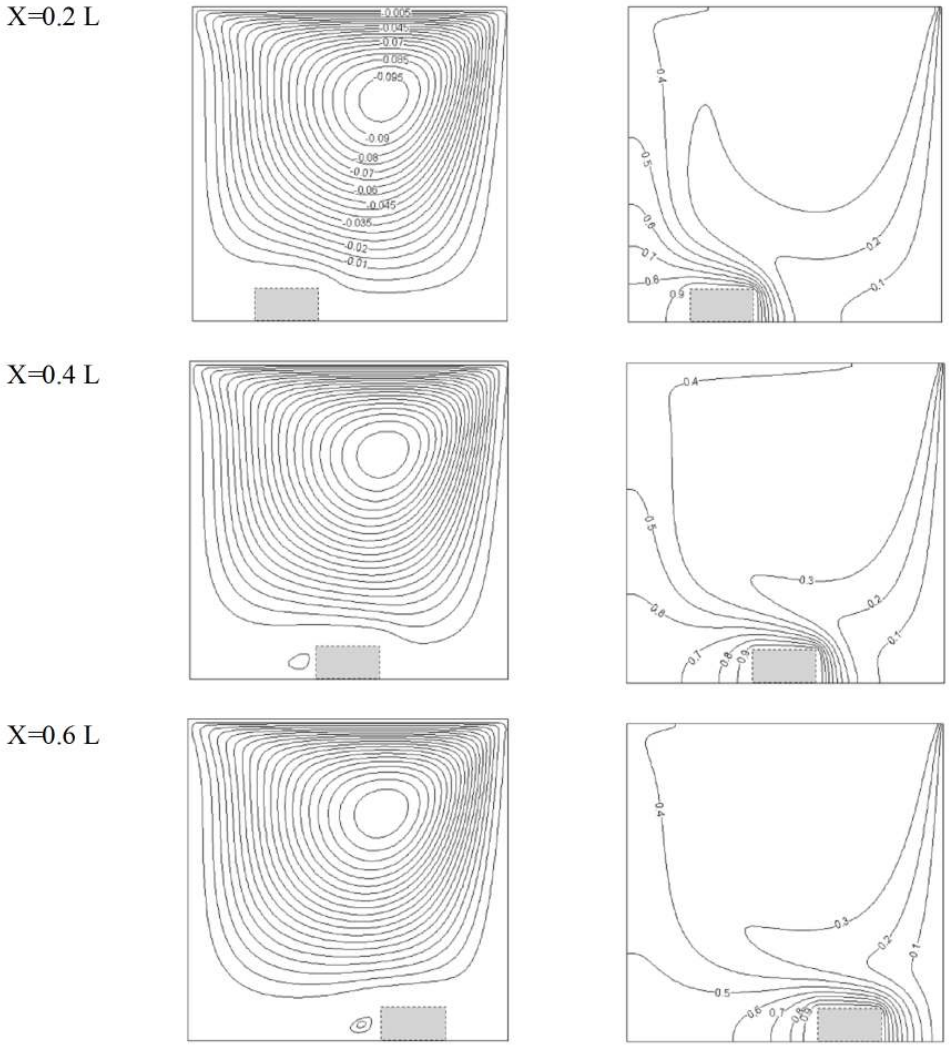

FIG. 5: Streamlines (on the left) and isotherms (on the right) at d_p = 40 nm, φ = 0.05, and T = 300° for different positions of the hot obstacle on the bottom wall

temperature gradient near the hot wall increases and therefore it is expected that heat transfer inside the cavity increases as the hot obstacle is moved further away from the left wall.

Diagram of the Nusselt number versus the Richardson number for different nanoparticle diameters is illustrated in Fig. 6. In this diagram it is assumed that $\varphi = 0.05$ and $x = 0.4L$. It is seen from this diagram that as the Richardson number increases and the buoyancy force starts to dominate the shear force, the Nusselt number and heat transfer inside the cavity decrease. On the other hand, using formulation of variable attributes in this research, it can be found that the size of nanoparticle diameter can influence the Nusselt number and heat transfer rate inside the cavity. As is seen, a general trend exists for the thermal behavior of the nanofluid at all Richardson numbers and different diameters. This trend indicates that the heat transfer rate at all Richardson numbers studied increases with a decreasing nanoparticle diameter.

Figure 7 shows variation of the mean Nusselt number as a function of the Richardson number for different distances of the obstacle from the left wall and at $\varphi = 0.05$ and $d_p = 40$ nm. In this range of parameters, an increasing Richardson number also causes the heat transfer rate inside the cavity to decrease. On the other hand, as the obstacle is moved further away from the left wall, the Nusselt number and heat transfer rate inside the cavity increase. This increase in the heat transfer rate is mostly related to the rotation of the primary cell and configuration of the obstacle upstream the flow.

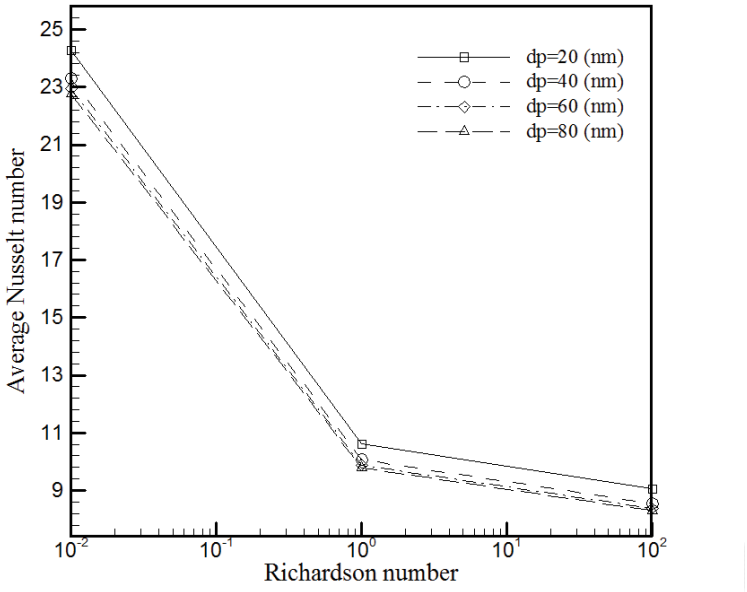

FIG. 6: Variation of the average Nu numbers with the Richardson number for $\varphi = 0.05$ and $d_p = 40$ nm and different d_p equal to 20 nm, 40 nm, 60 nm, and 80 nm

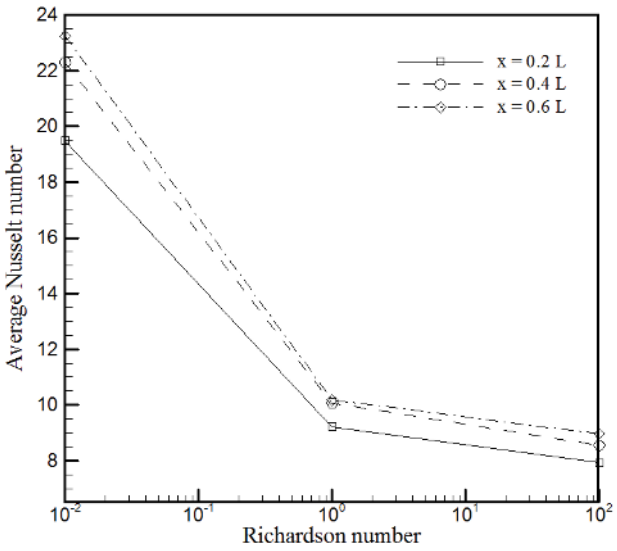

FIG. 7: Variation of the average Nu numbers with the Richardson number at φ = 0.05 and x = 0.4L and different positions of the hot obstacle

5. CONCLUSIONS

In this paper, the thermal characteristics, heat transfer, and flow patterns inside a cavity filled with a nanofluid and having a hot square obstacle were investigated. The effect of different parameters such as the average diameter of nanoparticles, Richardson number, and the position of obstacle on the bottom wall were studied and the following results were obtained by analyzing different diagrams and figures:

1) with an increasing Richardson number, the heat transfer rate and the Nusselt number decrease;

2) one of the important parameters that control heat transfer inside the cavity is the position of the hot obstacle on the bottom wall. The results indicate that changing the position of the hot obstacle causes up to an 18.9% (at low Ri) increase in the heat transfer rate;

3) as the nanoparticle diameter decreases, the isothermal lines near the isothermal walls become slightly crowded and therefore the heat transfer is enhanced.

REFERENCES

Abbasian Arani, A. A., Amani, J., and Hemmat Esfe, M., Numerical simulation of mixed convection flows in a square double lid-driven cavity partially heated using nanofluid, *J. Nanostruct*., vol. 2, pp. 301–311, 2012.

Abdelkhalek, M. M., Mixed convection in a square cavity by a perturbation technique, *Comput. Mater. Sci*., vol. 42, pp. 212–219, 2008.

Abu–Nada, E. and Chamkha, A. J., Mixed convection flow in a lid driven square enclosure filled with a nanofluid, *Eur. J. Mech. B Fluids*, vol. 29, pp. 472–482, 2010.

Cha, C. K. and Jaluria, Y., Recirculating mixed convection flow for energy extraction, *Int. J. Heat Mass Transfer*, vol. 27, pp. 1801–1810, 1984.

Chang, H., Jwo, C. S., Lo, C. H., Tsung, T. T., Kao, M. J., and Lin, H. M., Rheology of CuO nanoparticle suspension prepared by ASNSS, *Rev. Adv. Mater. Sci*., vol. 10, pp. 128–132, 2005.

Choi, S. U. S., Enhancing thermal conductivity of fluids with nanoparticles, developments and applications of non-Newtonian flows, in: D. A. Siginer and H. P. Wang (Eds.), FEDvol. 231/MDvol. 66, New York: The American Society of Mechanical Engineers, pp. 99–105, 1995.

Fereidoon, A., Saedodin, S., Hemmat Esfe, M., and Noroozi, M. J., Evaluation of mixed convection in inclined square lid driven cavity filled with Al_2O_3/water nanofluid, *Eng. Appl. Comput. Fluid Mech*., vol. 7, no. 1, pp. 55–65, 2013.

Hamilton, R. L. and Crosser, O. K., Thermal conductivity of heterogeneous two component systems, *Ind. Eng. Chem. Fund*., vol. 1, pp. 187–191, 1962.

Ideriah, F. J. K., Prediction of turbulent cavity flow driven by buoyancy and shear, *J. Mech. Eng. Sci*., vol. 22, pp. 287–295, 1980.

Imberger, J. and Hamblin, P. F., Dynamics of lakes, reservoirs, and cooling ponds, *Annu. Rev. Fluid Mech*., vol. 14, pp. 153–187, 1982.

Jang, S. P., Lee, J. H., Hwang, K.S., and Choi, S. U. S., Particle concentration and tube size dependence of viscosities of Al_2O_3–water nanofluids flowing through micro- and minitubes, *Appl. Phys. Lett*., vol. 91, pp. 24-31, 2007.

Khanafer, K. M., Al-Amiri, A. M., and Pop, I., Numerical simulation of unsteady mixed convection in a driven cavity, using an externally excited sliding lid, *Eur. J. Mech. B Fluids*, vol. 26, pp. 669–687, 2007.

Lee, S., Choi, S. U. S., Li, S., and Eastman, J. A., Measuring thermal conductivity of fluids containing oxide nanoparticles, *Int. J. Heat Mass Transfer*, vol. 121, pp. 280–289, 2001.

Mahmoodi, M. and Mazrouei Sebdani, S., Natural convection in a square cavity containing a nanofluid and an adiabatic square block at the center, *Superlattice Microstruct*., vol. 52, pp. 261–275, 2012.

Mahmoodi, M., Mixed convection inside nanofluid filled rectangular enclosures with moving bottom wall, *Thermal Sci*., vol. 15, no. 3, pp. 889–903, 2011.

Mazrouei Sebdani, S., Mahmoodi, M., and Hashemi, S. M., Effect of nanofluid variable properties on mixed convection in a square cavity, *Int. J. Thermal Sci*., vol. 52, pp. 112–126, 2012.

Moallemi, M. K. and Jang, K. S., Prandtl number effects on laminar mixed convection heat transfer in a lid-driven cavity, *Int. J. Heat Mass Transfer*, vol. 35, pp. 1881– 1892, 1992.

Nikfar, M. and Mahmoodi, M., Meshless local Petrov–Galerkin analysis of free convection of nanofluid in a cavity with wavy side walls, *Eng. Anal. Bound. Elem*., vol. 36, pp. 433–445, 2012.

Patel, H. E., Pradeep, T., Sundararajan, T., Dasgupta, A., Dasgupta, N., and Das, S. K., A micro convection model for thermal conductivity of nanofluid, *Pramana-J. Phys*., vol. 65, pp. 863–869, 2005.

Pilkington, L. A. B., Review lecture: the float glass process, *Proc. Roy. Soc. London A*, vol. 314, pp. 1–25, 1969.

Sadodin, S., Hemmat Esfe, M., and Noroozi, M. J., Numerical simulation of mixed convection of fluid flow and heat transfer within car radiator with an inside obstacle filled with nanofluid, *E-Model*., vol. 9, no. 25, pp. 33–46, 2011.

Sharif, M. A. R., Laminar mixed convection in shallow inclined driven cavities with hot moving lid on top and cooled from bottom, *Appl. Therm. Eng*., vol. 27, nos. 5–6, pp. 1036–1042, 2007.

Tiwari, R. K. and Das, M. K., Heat transfer augmentation in a two-sided lid-driven differentially heated square cavity utilizing nanofluids, *Int. J. Heat Mass Transfer*, vol. 50, pp. 2002–2018, 2007.

Waheed, M. A., Mixed convective heat transfer in rectangular enclosures driven by a continuously moving horizontal plate, *Int. J. Heat Mass Transfer*, vol. 52, pp. 5063–5055, 2009.

Xie, H. Q., Wang, J. C., Xi, T. G., Li, Y., and Ai, F., Dependence of the thermal conductivity of nanoparticle–fluid mixture on the base fluid, *J. Mat. Sci. Lett*., vol. 21, pp. 1469–1471, 2002.

Xu, J., Yu, B., Zou, M., and Xu, P., A new model for heat conduction of nanofluids based on fractal distributions of nanoparticles, *J. Phys. D*, vol. 39, pp. 4486–4490, 2006.

Xuan, Y. and Li, Q., Investigation on convective heat transfer and flow features of nanofluids, *J. Heat Transfer*, vol. 125, pp. 151–155, 2003.

Zarei, H., Rostamian, S. H., and Hemmat Esfe, M., Heat transfer behavior of mixed convection flow in lid driven cavity containing hot obstacle subjected to Nanofluid with variable properties, *J. Basic Appl. Sci. Res*., vol. 3, no. 2, pp. 713–721, 2013.